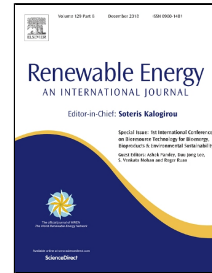


Accepted Manuscript

Investigation on long-term extreme response of an integrated offshore renewable energy device with a modified environmental contour method

Liang Li, Zhi-Ming Yuan, Yan Gao, Xinshu Zhang, Tahsin Tezdogan



PII: S0960-1481(18)30935-2
DOI: 10.1016/j.renene.2018.07.138
Reference: RENE 10412
To appear in: *Renewable Energy*
Received Date: 02 November 2017
Accepted Date: 29 July 2018

Please cite this article as: Liang Li, Zhi-Ming Yuan, Yan Gao, Xinshu Zhang, Tahsin Tezdogan, Investigation on long-term extreme response of an integrated offshore renewable energy device with a modified environmental contour method, *Renewable Energy* (2018), doi: 10.1016/j.renene.2018.07.138

This is a PDF file of an unedited manuscript that has been accepted for publication. As a service to our customers we are providing this early version of the manuscript. The manuscript will undergo copyediting, typesetting, and review of the resulting proof before it is published in its final form. Please note that during the production process errors may be discovered which could affect the content, and all legal disclaimers that apply to the journal pertain.

Investigation on long-term extreme response of an integrated offshore renewable energy device with a modified environmental contour method

Liang Li^a, Zhi-Ming Yuan^{a*}, Yan Gao^a, Xinshu Zhang^b, Tahsin Tezdogan^a

^a*Department of Naval Architecture, Ocean and Marine Engineering, University of Strathclyde, UK*

^b*School of Naval Architecture, Ocean and Civil Engineering, Shanghai Jiao Tong University, China*

Abstract

Considering the massive simulations required by the full long-term analysis, the environmental contour method is commonly used to predict the long-term extreme responses of an offshore renewable system during life time. Nevertheless, the standard environmental contour method is not applicable to the wind energy device due to the non-monotonic aerodynamic behaviour of the wind turbine. This study presents the development of a modified environmental counter method and its application to the extreme responses of a hybrid offshore renewable system. The modified method considers the variability of the responses by checking multiple contour surfaces so that the non-monotonic aerodynamic behaviour of the wind turbine is considered. The hybrid system integrates a floating wind turbine, a wave energy converter and two tidal turbines. Simulation results prove that the modified method has a better accuracy. *Keywords:* extreme response, environmental contour method, renewable energy, floating wind turbine, wave energy converter, tidal turbine

1. Introduction

Powered by the increasing global pursuit of offshore renewable energy, various types of ocean energy systems are developed, including the floating wind turbine, the wave energy converter and the tidal turbine. Studies on an individual energy system have been fully conducted [1-5]. Nevertheless, producing power from a single type of ocean energy resource faces the problem of high cost and low harvesting efficiency. Therefore, the concept of integrated offshore renewable energy devices is proposed.

Nehrir et al. [6] presented a review of hybrid renewable energy systems, in term of configurations, control and applications. Aubault et al. [7] incorporated an oscillating-water-column WEC into a semi-submersible floating wind turbine. They showed that the overall cost could be reduced by sharing the mooring system and the power infrastructure. Muliawan et al. [8] studied the dynamic response and the power performance of the so-called STC concept in various operational conditions. Their simulation results revealed a synergy between wind and wave energy generation. Experimental and numerical

* Corresponding author at: Dep. of Naval Architecture, Ocean & Marine Engineering, University of Strathclyde.

Henry Dyer Building, G4 0LZ, Glasgow, UK.

Tel: + 44 (0)141 548 3308

E-mail address: zhiming.yuan@strath.ac.uk

31 studies of the STC in survival mode were conducted by Wan et al. [9, 10]. Wan et al. [11] investigated
32 the hydrodynamic responses of STC under operational conditions. Michailides et al. [12] incorporated
33 a flap-type WEC to a semi-submersible floating wind turbine and investigated the effect of WECs on
34 the response of the integrated system. Their study showed that the combined operation of the rotating
35 flaps resulted in an increase of the produced power without affecting the critical response quantities of
36 the semi-submersible platform significantly. Li et al. [13] proposed a hybrid offshore renewable energy
37 device by combining a floating wind turbine, a WEC and two tidal turbines. It was shown that the
38 overall power production was increased while the platform motions were reduced. The short-term
39 extreme response of this concept was further examined by Li et al. [14]. Bachynski and Moan [15]
40 studied the effects of three point-absorber WECs on a TLP floating wind turbine in operational and 50-
41 year extreme environmental conditions, in terms of power production, structural loads and platform
42 motions.

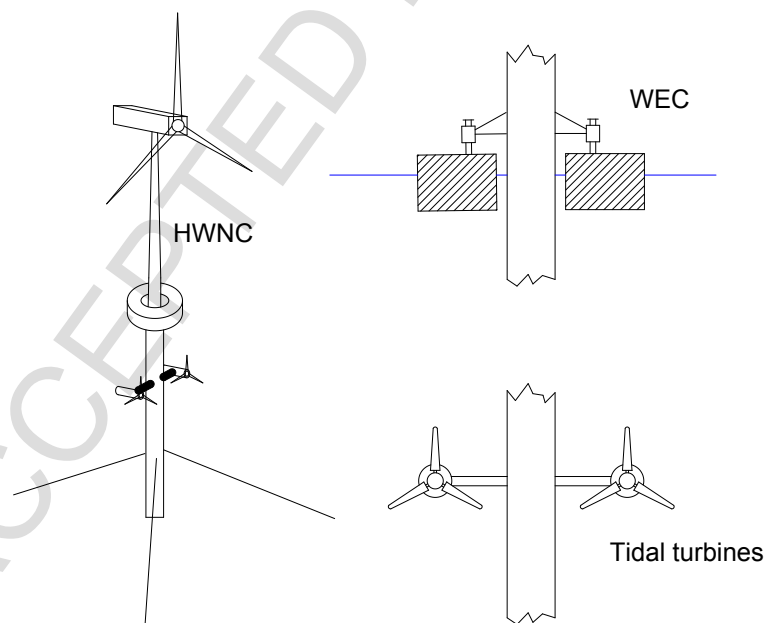
43 For the design of offshore renewable energy devices, a long-term analysis is necessary to estimate
44 the life-time fatigue damage and the extreme structural responses. The long-term analysis integrates the
45 short-term response with a given environmental distribution model to value the life-time values, which
46 is the basic idea of the so-called full long-term analysis (FLTA). Coe et al. [16] performed a full long-
47 term analysis on the dynamic responses of a WEC. Agarwal and Manuel [17] investigated the extreme
48 response of an offshore floating wind turbine with the FLTA. Nevertheless, the FLTA requires massive
49 simulations of short-term response to cover every combination of environmental parameters. It is
50 inefficient and many alternative methods have been developed. Videiro and Moan [18] proposed a
51 simplified FLTA method which assumed that only the environmental conditions around a critical
52 condition have influence on the extreme responses. Winterstein et al. [19] introduced an inverse first-
53 order reliability method (IFORM). In their method, the uncertainties in the gross environment condition
54 and the extreme response given the environment condition were decoupled. The IFORM is based on
55 the transformation between a standardized normal space and a physical space (in which the variables
56 are response and environmental parameters). All the possible combinations of variables at given a return
57 period are firstly identified in the normal space and transformed back to the physical space again. The
58 critical environmental condition is selected from contour surfaces, which are the combinations of
59 transformed variables. Xiang and Liu [20] used the IFORM to predict the probabilistic fatigue life. A
60 further simplification of the IFORM is the so-called environmental contour method (ECM), which
61 ignores the variability of the response and assumes that the critical environmental condition is located
62 on the N -year contour surface. As not many simulation realizations are required, the ECM have been
63 widely used to estimate the extreme response induced by wave loads. Li et al. [21] investigated the
64 extreme response of a bottom-fixed offshore wind turbine. The contour surface corresponding to a so-
65 called important wind speed is used to collect the critical environmental condition. Karmakar et al. [22]
66 used the ECM to predict the long-term load of a spar and a semisubmersible floating wind turbine.
67 Canning et al. [23] perform a long-term reliability analysis of a wave energy converter with ECM.

68 Nevertheless, for the response of a floating wind turbine the ECM may be not applicable due to the
 69 monotonic performance of wind force and the complete IFORM without omission of the response
 70 should be used. This problem has been reported in previous studies [24-26].

71 In this study, a modified environmental contour method is proposed to estimate the long-term
 72 extreme response of offshore renewable energy system. The modified method considers the variability
 73 of the response by checking multiple environmental contours of different return periods. In this way,
 74 the non-monotonic behaviour of wind turbine is covered. The modified method is used to estimate the
 75 50-year extreme response of a hybrid offshore renewable energy system. The hybrid system is based
 76 on the combination of a floating wind turbine, a WEC and two tidal turbines.

77 2. Model description

78 The hybrid concept addressed in this study, namely ‘HWNC’ (Hywind-Wavebob-NACA_638xx
 79 Combination, see Fig. 1), is based on the combination of the spar type floating wind turbine Hywind
 80 [27], the two-body floating WEC ‘Wavebob’ and two tidal turbines with tidal turbines with
 81 NACA_638xx airfoil series. The WEC, designed to move only in heave mode relative to the platform
 82 while no relative surge, sway, roll, pitch and yaw motions are allowed, is connected to the platform
 83 through mechanical facilities. Two tidal turbines are installed to harvest energy from the sea current.
 84 The main dimensions of the HWNC concept are presented in Table 1 and the inertial properties of each
 85 component are listed in Table 2.



86
 87 Fig. 1. HWNC concept.
 88
 89

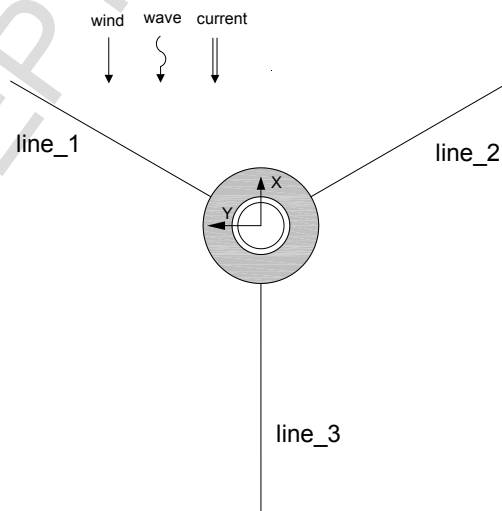
90 Table 1
91 Main dimensions of the HWNC.

	Item	Value
Platform	Draft	120 m
	Tower base above still water level (SWL)	10 m
	Depth to top of taper below SWL	4 m
	Depth to bottom of taper below SWL	12 m
	Platform diameter above taper	6.5 m
	Platform diameter below taper	9.4 m
WEC	Draft	4 m
	Outer diameter	20 m
	Inner diameter	10 m
Tidal turbine	Depth below SWL	46.5 m
	Rotor diameter	10 m

92
93 Table 2
94 Inertial properties of subsystem.

	Item	Value
Platform	Total mass	6,995,130 kg
	Centre of mass (CM) below SWL	89.9 m
	Roll inertia about CM	4,229,230,000 kg·m ²
	Pitch inertia about CM	4,229,230,000 kg·m ²
	Yaw inertia about CM	164,230,000 kg·m ²
WEC	Total mass	1,442,000 kg
	CM below SWL	0 m
	Roll inertia about CM	3,139,900 kg·m ²
	Pitch inertia about CM	3,139,900 kg·m ²
	Yaw inertia about CM	6,022,200 kg·m ²

95
96 The HWNC is operated at sea site with a water depth of 320 m and moored by three slack catenary
97 lines. The fairleads are connected to the platform at 70 m below the still water level. Fig. 2 displays the
98 configuration of the mooring system. The three lines are oriented at 60°, 180°, and 300° about the
99 vertical axis. The relevant properties of the mooring lines are listed in Table 3.



100
101

Fig. 2. Configuration of mooring lines.

102 Table 3
103 Mooring line properties.

Item	Value
Depth to anchors	320 m
Depth of fairleads	70 m
Radius to anchors	853.87 m
Radius to fairleads	5.2 m
Unstretched mooring line length	902.2 m
Mooring line diameter	0.09 m
Equivalent mooring line mass density	77.7066 kg/m
Equivalent mooring line extensional stiffness	384,243,000 N

104

105 3. Numerical model and validation

106 3.1. *modelling*

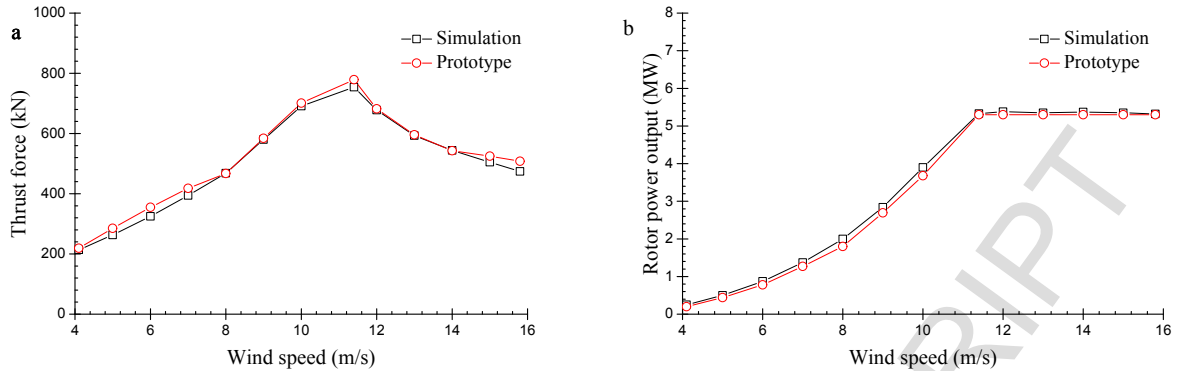
107 The numerical code used to perform the coupled simulation in this work is based on the combination
108 of WindSloke developed by Li et al. [28] and WEC-Sim [29] developed under the collaboration
109 between the National Renewable Energy Laboratory (NREL) and the Sandia National Laboratories.
110 The aerodynamic module of WindSloke is used in this work to calculate the unsteady wind turbine
111 thrust force by a modified blade element momentum (BEM) method. The same method is used to
112 compute the tidal turbine thrust forces. The unsteadies of the inflow caused by platform motions is
113 considered with a dynamic wake model [30]. WEC-Sim is a wave energy converter simulation tool with
114 the ability to model offshore systems that are comprised of rigid bodies, PTO systems and mooring
115 systems. WEC-Sim computes the hydrodynamic forces acting on the floating bodies based on the
116 combination of potential flow theory and Morison equation.

117 Three rigid bodies are established in the numerical model of the HWNC. The spar platform and the
118 WEC are treated as two independent floating bodies and their hydrodynamic interactions are considered.
119 The two components are connected by the PTO facility, which is numerically treated as a spring &
120 damper system. The stiffness coefficient K is set to 5 kN and the damping coefficient B is set to 80
121 kN·s/m. The wind turbine is regarded as a non-hydro body, which is rigidly mounted on the platform.
122 Please note that deflection of the tower is not considered in this study. The mooring line is modelled
123 with the lumped-mass approach, which divides the mooring line into a series of evenly-sized segment
124 represented by connected nodes and spring & damper systems. The lumped-mass approach merely
125 models the axial properties of the mooring lines while the torsional and bending properties are neglected.
126 The effects of wave kinematics and any other external loads on the lines are also ignored in the lumped-
127 mas model.

128 3.2. *Validation*

129 Since the thrust forces acting on the wind turbine and the tidal turbines are simulated with the same
130 approach, only aerodynamic force is validated here. Firstly, the steady aerodynamic performance of the

131 wind turbine is simulated. Fig. 3 displays the steady aerodynamic performance of the wind turbine, in
 132 terms of thrust force and rotor power output.



133

134

Fig. 3. Aerodynamic performance of the wind turbine. (a) thrust force; (b) rotor power output.

135 For a floating wind turbine, the wind force acting on the rotor is unsteady due to the aero-hydro
 136 couplings. To validate the unsteady aerodynamic performance, the wind turbine thrust force is
 137 simulated under a set of sinusoidal winds and the simulation results are compared with those obtained
 138 by FAST (version v7.02.00d-bjj) [31]. The speed of sinusoidal wind is defined by

139

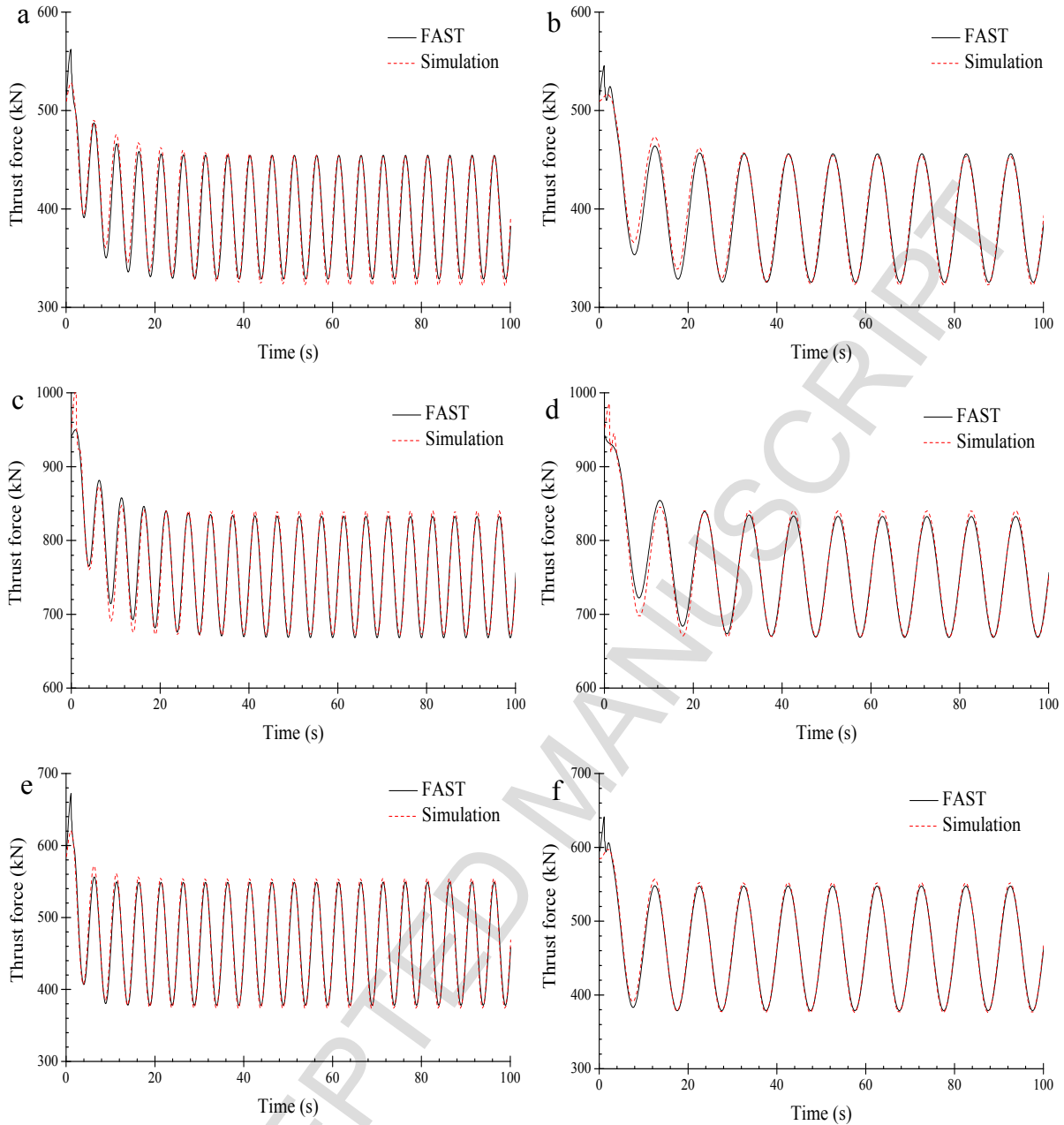
$$V(t) = V_0 + \sin(\omega t) \quad (1)$$

140

141

142

where V_0 is the mean wind speed and ω is the varying frequency. The control module in FAST is
 switched off so that the rotor speed and the blade pitch angle are fixed in the simulations. Fig. 7 displays
 time series of the unsteady wind turbine thrust forces predicted by the simulation tool and FAST.



143

144

145

146

Fig. 4. Times series of unsteady wind turbine thrust forces. (a) $V_0=8$ m/s, $\omega=1.26$ rad/s; (b) $V_0=8$ m/s, $\omega=0.63$ rad/s; (c) $V_0=11.4$ m/s, $\omega=1.26$ rad/s; (d) $V_0=11.4$ m/s, $\omega=0.63$ rad/s; (e) $V_0=14$ m/s, $\omega=1.26$ rad/s; (f) $V_0=14$ m/s, $\omega=0.63$ rad/s.

147

148

149

150

151

152

153

154

The model test of a spar type floating wind turbine conducted by Koo et al. [32] is used to validate the numerical modelling of aero-hydro couplings. The spar type floating wind has an identical platform geometry with the Hywind, despite that the mass and inertia of the platform were changed (see Table 4). Furthermore, the mooring system was also somewhat varied (see Table 5). Please refer to [32] for more details of the model test set-up. The numerical model of the floating wind turbine used by Koo et al. [32] is developed and the simulation results are compared with the model test measurement to validate the aero-hydro couplings. White noise waves were generated in the model test to get the response amplitude operator (RAO) of platform motions in the presence of rated wind turbine thrust

155 force. The same procedure is employed in the numerical simulation. Fig. 5 compares the RAOs acquired
156 by the simulation tool and the experiment.

157 Table 4

158 Mass property of the platform in [32].

Item	Value
Mass	7,980,000 kg
Roll gyration	53.54 m
Pitch gyration	53.54 m
Yaw gyration	3.68 m

159

160 Table 5

161 Mooring system in [32]

Item	Value
Anchor radius	445 m
Anchor depth	200 m
Fairlead radius	5.2 m
Fairlead depth	70 m

162

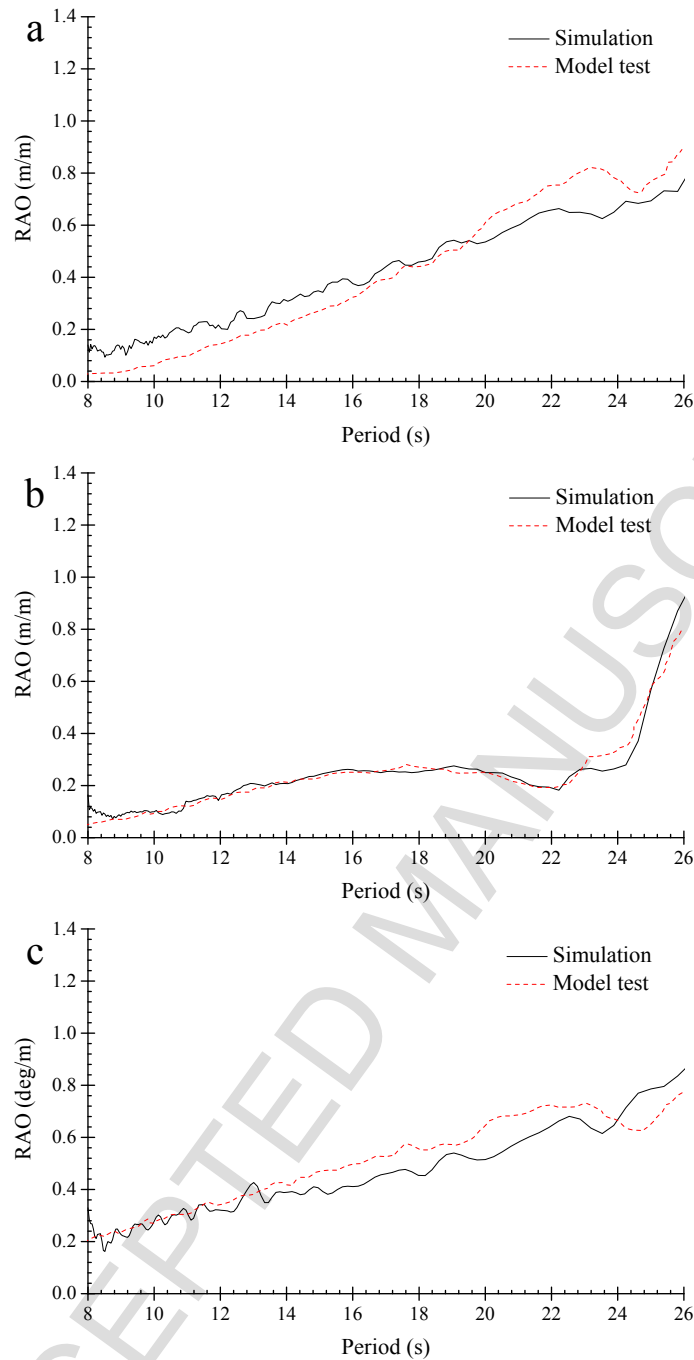


Fig. 5. RAOs of platform motions. (a) surge motion; (b) heave motion; (c) pitch motion.

163

164

165 4. Long-term extreme analysis

166 4.1. Full long-term analysis

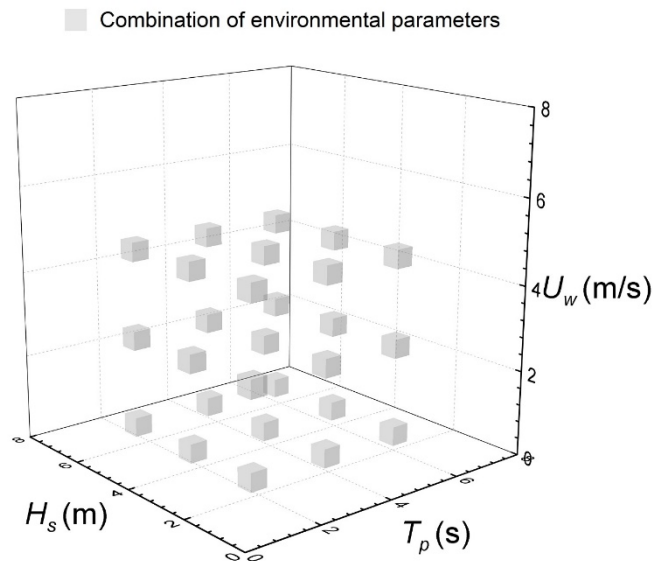
167 The full long-term analysis method is a very straightforward approach to predict the extreme
 168 response, which considers all the combinations of environmental condition parameters (see Fig. 6). The
 169 FLTA method calculates the long-term cumulative distribution function (CDF) just by integrating the
 170 short-term probability functions and the corresponding environmental condition parameters

$$171 \quad F_X^{LT}(x) = \int F_{X|S}^{ST}(x|s) f_S(s) ds \quad (2)$$

172 where x is response variable and s is the environmental condition parameter. F_X^{LT} is the long-term CDF
 173 of response while $F_{X|S}^{ST}$ is the short-term CDF at a given environmental condition s . f_S is the probability
 174 density function used to describe the environmental condition. In this study, we use the 1-hr short-term
 175 CDF to extrapolate the 50-year long-term extreme response. Since wind speed u , wave height h and
 176 wave period t is the dominating environmental parameters, Eq. (2) can be re-written as

$$177 \quad F_{X_{50\text{-year}}}^{LT}(x) = \left[F_{X_{1\text{-hr}}}^{LT}(x) \right]^{50 \times 365.25 \times 24} \quad (3)$$

$$F_{X_{1\text{-hr}}}^{LT}(x) = \iiint F_{X_{1\text{-hr}}|U,H,T}^{ST}(x|u,h,t) f_{U,H,T}(u,h,t) du dh dt$$



178
 179 Fig. 6. Combinations of environmental parameters.

180 4.2. Modified environmental contour method

181 As shown in Eq. (3), the FLTA method requires massive simulations and it can be extremely time
 182 consuming. Therefore, simplified methods have been developed to enhance the efficiency. The
 183 environmental contour method is one of these methods, which is based on the IFORM and assumes that
 184 the long-term extreme values are just affected by several critical environmental conditions. The ECM
 185 aims at selecting the most important environmental condition, namely the essential combination of
 186 environmental parameters, located on the contour surface with a desired N -year return period.

$$187 \quad F_{X_{1\text{-hr},N\text{-year}}}^{LT} \approx F_{X_{1\text{-hr}}|U_w,H_s,T_p}^{ST}(x|u_N, h_N, t_N) \quad (4)$$

188 (u_N, h_N, t_N) is the environmental parameter leading to the largest extreme response in the N -year return
 189 period contour surface. The generation of the environmental contour surface is based on the Rosenblatt
 190 transformation, which transforms the environmental parameter X from the initial X -space into a
 191 nonphysical U -space (see Fig. 7).

$$192 \quad U = T_2(T_1(X)) \quad (5)$$

193

$$T_1 : Y = \begin{pmatrix} F_1(x_1) \\ \dots \\ F_{k|1,\dots,k-1}(x_k | x_1, \dots, x_{k-1}) \\ \dots \\ F_{n|1,\dots,n-1}(x_n | x_1, \dots, x_{n-1}) \end{pmatrix} \quad (6)$$

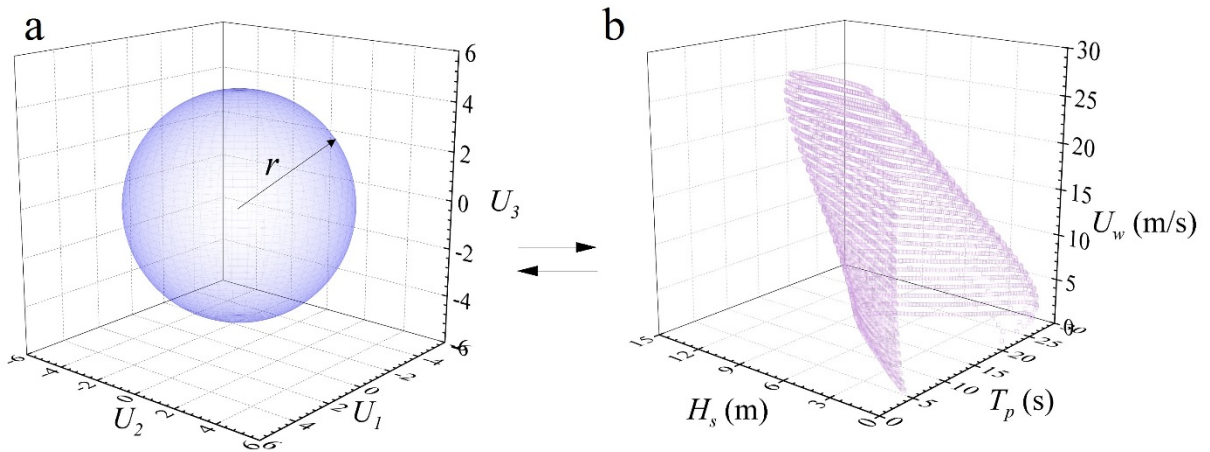
194

$$T_2 : U = \begin{pmatrix} \Phi^{-1}(y_1) \\ \dots \\ \Phi^{-1}(y_k) \\ \dots \\ \Phi^{-1}(y_n) \end{pmatrix} \quad (7)$$

195 Φ is CDF of the standard normal distribution. In the U-space, all combinations of transformed
 196 environmental parameters with respect to N-year return period are located on a sphere with radius r

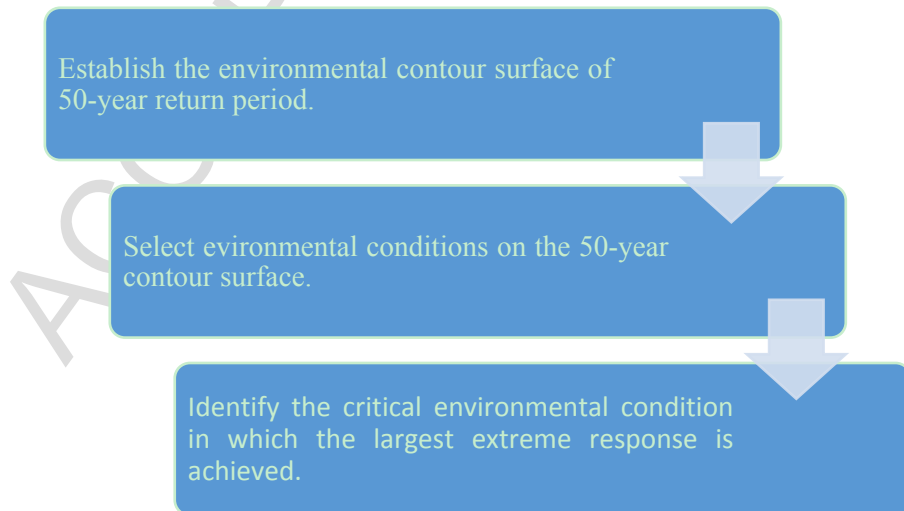
197

$$r = \Phi^{-1}\left(1 - \frac{1}{N \times 365.25 \times 24}\right) \quad (8)$$



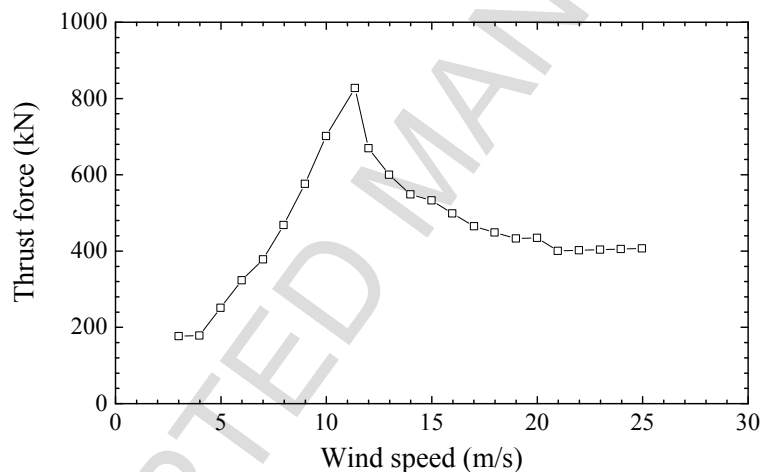
198
 199 Fig. 7. Rosenblatt transformation. (a) U-space; (b) X-space.

200 Then the environmental contour surface can be obtained by transforming the sphere back to the U-
 201 space. The procedures of ECM are outlined in Fig. 8.



202
 203 Fig. 8. Procedures of ECM.

204 The above discussions outline the basic procedures of ECM, which is actually a simplification of
 205 IFORM, ignoring the variability of response and decoupling the response variability and the
 206 environment. It inherently implies that the ECM assumes the actual critical environmental condition to
 207 be close to the counter surface in X-space or the sphere in U-space with respect to the 50-year return
 208 period. Due to this assumption, which is also the limitation of ECM, ECM is not applicable to a floating
 209 wind turbine [24, 25]. This is because the wind force is not monotonic with the wind speed, especially
 210 around the cut-out wind speed. As shown in Fig. 9, the thrust force reaches the maximum value at rated
 211 wind speed (11.4 m/s) and drops gradually as the wind speed continues increasing. If the wind speed
 212 exceeds the cut-out speed 25 m/s, the wind turbine is parked and no wind force is applied on the rotor.
 213 In this case, the responses induced by wind force are higher in operational state and lower in parked
 214 state. Moreover, a discontinuity appears at 25 m/s. Consequently, the omission of response variability
 215 is not reasonable. In this circumstance, the IFORM should be used. Although the IFORM is already a
 216 simplification than the FLTA, it is still more complex than the ECM and requires massive simulations.
 217 Therefore, a modification is made to the ECM in this study, which considers the variability of response
 218 by checking multiple environmental contour surfaces.



219

220

Fig. 9. Relationship between thrust force and wind speed at hub height.

221 Basically, the procedures of the modified ECM is similar with those of the EMC, which can be
 222 regarded as an expansion of the ECM while still a simplification of the IFORM. The main idea of the
 223 modified ECM is to include multiple important contour surfaces rather than the 50-year one alone. As
 224 shown in Fig. 10, the first step is to select a set of wind speeds with respect to different return periods
 225 and the corresponding most probable wave heights and wave periods based on a joint wind-wave
 226 distribution model. Simulations are afterwards performed to acquire the extreme values with respect to
 227 these selected environmental parameters. The first step is introduced to find the wind speed in which
 228 the non-monotonic behaviour of the wind turbine is the most significant. Subsequently, the N -year
 229 return period corresponding to a response peak as well as the 50-year return period are selected. A
 230 response peak is observed because the non-monotonic behaviour of the wind turbine is remarkable at
 231 this wind speed. It should be noted that the wind speed at 10 m above the mean sea level is used to

232 represent the environmental conditions in this study, therefore the cut-out speed measured in Fig. 10 is
 233 not 25 m/s (the cut-out wind speed 25 m/s refers to hub height). The hub height wind speed is not used
 234 because the joint wind-wave wave probability distribution model used in this study is only applicable
 235 to wind speed at 10 m height. Finally, search for the critical environmental condition on the selected
 236 multiple contour surfaces (including the 50-year one). In this way, the variability of response is
 237 considered by checking multiple contour surfaces with different return periods. If all the contour
 238 surfaces within 50-year return period is included, then the modified ECM will become the IFORM. If
 239 only the 50-year contour surface is identified (no response peak occurs), the modified ECM becomes
 240 the ECM.

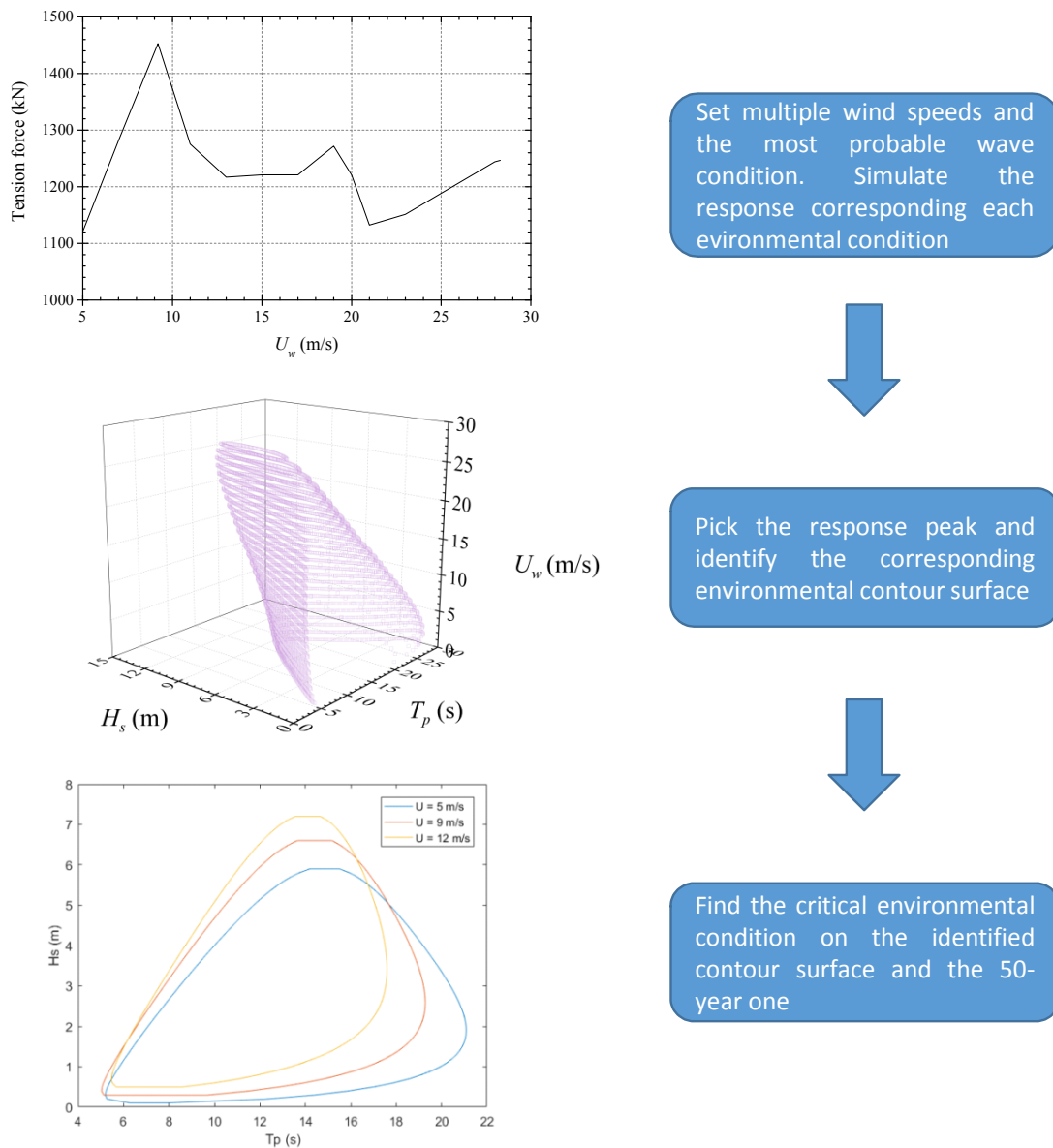


Fig. 10. The procedure of modified ECM.

243 For an N -year return period identified by the modified ECM, assuming each 1-hr period is
 244 independent, the 1-hr extreme CDF of N -year return period can be used to extrapolate the 1-hr extreme
 245 CDF of 50-year return period

$$246 \quad F_{X_{1-hr,50-year}}^{LT}(x) = \left[F_{X_{1-hr,N-year}}^{LT}(x) \right]^{50/N} \approx \left[F_{X_{1-hr}|U_w, H_s, T_p}^{ST}(x|u_N, h_N, t_N) \right]^{50/N} \quad (9)$$

247 As illustrated by Eq. (9), the modified ECM uses the 1-hr short-term CDF to approximate the 1-hr
 248 long-term CDF of N -year and then extrapolate it to acquire the 1-hr long-term CDF of 50-year return.
 249 Comparatively, the standard ECM merely use the 1-hr short-term CDF to get the 50-year extreme values.
 250 The two methods are identical if only the 50-year contour surface is identified.

251 Given that the critical environmental condition has been identified by the modified ECM, a certain
 252 amount of simulations is required to extrapolate the $F_{1-hr, N-year}^{LT}$. Assuming that the extreme response
 253 of an offshore structure converges to the Gumbel distribution

$$254 \quad F(x) = \exp(-\exp(-(x - \mu) / \sigma)) \quad (10)$$

255 Then the most probable 50-year extreme value is given by Eq. (11). In the following part of this paper,
 256 the extreme response refers to the most probable 50-year extreme response unless a special
 257 announcement is made.

$$258 \quad M_{X_{1-hr,50-year}} = \mu + \sigma \cdot \ln(50 / N) \quad (11)$$

259 One way to examine whether sufficient simulation realizations are performed is to check the 95%
 260 confidence interval. Assuming that the errors of the extreme values are normal distributed, the
 261 confidence interval is given by

$$262 \quad \begin{aligned} M_{CI\pm}(n) &= \hat{M}(n) + t_{2.5\%,n} \sqrt{\text{var}(\hat{M}(n)) / n} \\ \hat{M}(n) &= \hat{\mu}(n) + \hat{\sigma} \ln(50 / N) \end{aligned} \quad (12)$$

263 where $\hat{\mu}$ and $\hat{\sigma}$ are the estimated parameters of the Gumbel distribution based on n simulation
 264 realizations. $t_{2.5\%,n}$ is the 97.5% factile value Student's t -distribution with n degrees of freedom. A
 265 parameter CI is introduced to value whether the number of realizations is sufficient

$$266 \quad CI(n) = \frac{\hat{M}_{CI+}(n) - \hat{M}_{CI-}(n)}{\hat{M}(n)} \quad (13)$$

267 It is found that estimating μ and σ by Eq. (10) directly requires a huge amount of simulation
 268 realizations to acquire satisfactory approximation. Therefore, Eq. (10) is transformed to a linear
 269 equation and rewritten by Eq. (14). Fig. 11 displays the estimation of parameters μ and σ for mooring
 270 line tension force.

$$271 \quad x = \sigma \left\{ -\ln \left[-\ln(F) \right] \right\} + \mu \quad (14)$$

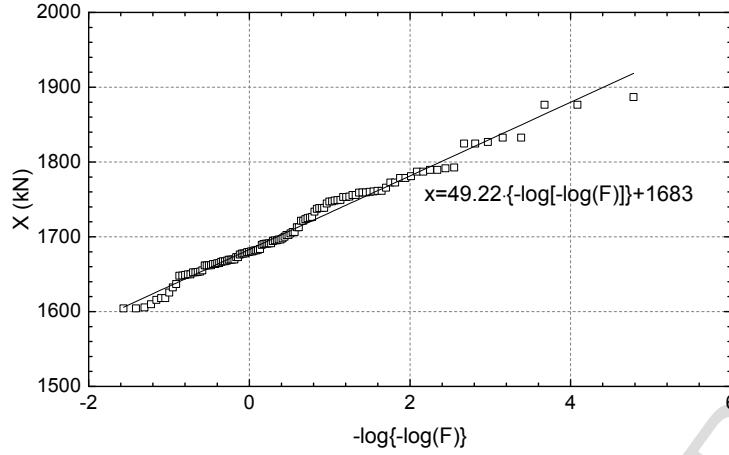


Fig. 11. Estimation of parameters μ and σ for mooring line tension force.

Different numbers of simulation realizations are checked and the results are listed in Table 6. As shown, 120 simulation realizations are sufficient to produce reliable prediction. Therefore, the following extreme responses presented in this study are based on 120 simulation realizations.

Table 6
CI with different number of simulations realizations.

n	Shear force (kN)	Bending moment (kN·m)	Tension force (kN)
80	1.6%	2.5%	1.4%
120	1.3%	2.1%	1.1%

4.3. Joint wind wave probability distribution model

The joint wind-wave distribution model developed by Li et al. [21] is used in this study. The model is based on the filed measurement in the North Sea centre from 2001 to 2010, which consists of a marginal distribution of wind speed at 10 m above the mean sea level U_w , a conditional distribution of wave height H_s given U_w , and a conditional distribution of wave period T_p given U_w and H_s ,

$$f_{U_w, H_s, T_p}(u, h, t) = f_{U_w}(u) \cdot f_{H_s|U_w}(h|u) \cdot f_{T_p|U_w, H_s}(t|u, h) \quad (15)$$

The wind speed follows the Weibull distribution

$$f_{U_w}(u) = \frac{\alpha_U}{\beta_U} \left(\frac{u}{\beta_U} \right)^{\alpha_U - 1} \cdot \exp \left[- \left(\frac{u}{\beta_U} \right)^{\alpha_U} \right] \quad (16)$$

The conditional wave height also converges to the Weibull distribution

$$f_{H_s|U_w}(h|u) = \frac{\alpha_H}{\beta_H} \left(\frac{u}{\beta_H} \right)^{\alpha_H - 1} \cdot \exp \left[- \left(\frac{u}{\beta_H} \right)^{\alpha_H} \right] \quad (17)$$

$$\alpha_H = a_1 + a_2 \cdot u^{a_3}$$

$$\beta_H = b_1 + b_2 \cdot u^{b_3}$$

Given a combination of U and H , the wave period converges to the log-normal distribution

$$f_{T_p|U_w, H_s}(t|u, h) = \frac{1}{\sqrt{2\pi}\sigma_{\ln(T)}t} \cdot \exp\left[-\frac{1}{2}\left(\frac{\ln(t) - \mu_{\ln(T)}}{\sigma_{\ln(T)}}\right)^2\right]$$

$$\mu_{\ln(T)} = \ln\left(\frac{\mu_T}{\sqrt{1+v_T^2}}\right), \sigma_{\ln(T)} = \sqrt{\ln(v_T^2 + 1)} \quad (18)$$

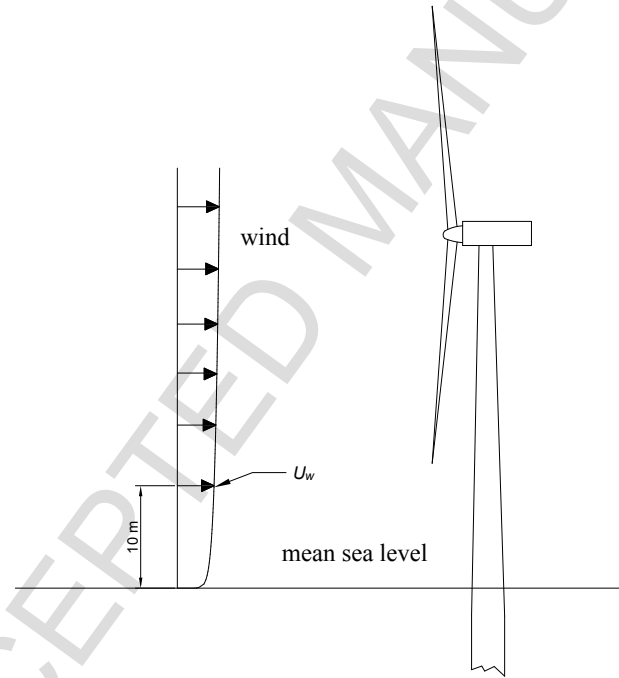
$$\mu_T = \bar{t}(h) \cdot \left[1 + \theta \left(\frac{u - \bar{u}(h)}{\bar{u}(h)}\right)^\gamma\right], v_T = k_1 + k_2 \cdot \exp(hk_3)$$

$$\bar{t}(h) = e_1 + e_2 \cdot h^{e_3}, \bar{u}(h) = f_1 + f_2 \cdot h^{f_3}$$

292 The parameters that used to specify the joint distribution model can be found in [21].

293 In a realistic sea site, the wind speed varies with the height so that the blades will experience different
294 wind speeds due to the rotor rotation (see Fig. 12). To calculate the wind force realistically, a power
295 law profile with exponent α equal to 0.1 is used to describe the wind speeds at different heights.

$$U_z(z) = U_w \cdot \left(\frac{z}{10}\right)^\alpha \quad (19)$$



297
298 Fig. 12. Wind profile.

299 5. Simulation and results

300 This section will examine the extreme response of the HWNC with the modified environmental
301 contour method proposed in this study.

302 The fore-aft tower base bending moment is firstly measured. Fig. 13 shows the first step of the
303 modified ECM. Generally, the behaviour of the bending moment is monotonic despite that a tiny
304 response peak is observed at $U_w = 9.2$ m/s (corresponding to 11.4 m/s at hub height). It can be simply
305 explained by that the response is governed by both wind force and wave load and thereby a response

306 peak appears when the wind turbine thrust force reaches maximum value at rated wind speed. According
 307 to the variation trend, wave load plays a more important role than the wind force. Based on the first step
 308 of the modified ECM, two contour surfaces are selected. The identified critical environmental condition
 309 and the extreme response are listed in Table 7. Since the critical condition selected by the two methods
 310 is located on the 50-year contour surface, it is obvious that the two methods predict identical extreme
 311 response. As discussed in Section 4.2, the ECM is valid when the wave loads play the dominating role,
 312 on which condition the critical environmental condition is close to the 50-year contour surface.
 313 Therefore, inclusion of environmental conditions from other contour surfaces will not increase the
 314 accuracy.

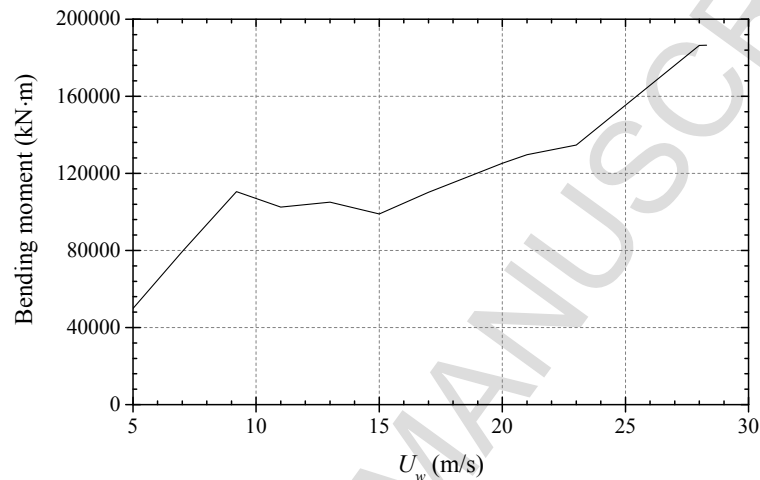


Fig. 13. Selection of contour surface.

315
316
317

318 Table 7
319 Selected critical environmental conditions and extreme bending moment

Method	Selected environmental parameters			Return period (year)	Extreme (kN·m)
	U_w (m/s)	H_s (m)	T_p (s)		
modified ECM	24.5	11.98	13.6	50	2.53×10^5
ECM	24.5	11.98	13.6	50	2.53×10^5

320

321 Mooring line 2 is selected as another representation of the structural response. The 1-hr extreme
 322 tension force with a return period of 50 years is investigated. As shown in Fig. 14, two response peaks
 323 are observed around $U_w = 9.2$ m/s and $U_w = 19$ m/s. Therefore, three contour surfaces are included in
 324 the modified ECM. Apparently, the wind force dominates the response and the non-monotonic
 325 behaviour of the response is quite notable, implying that the assumption of ECM is violated.

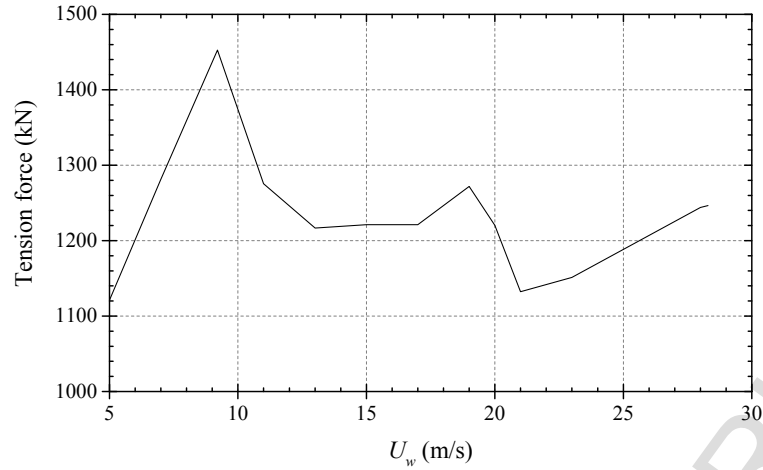
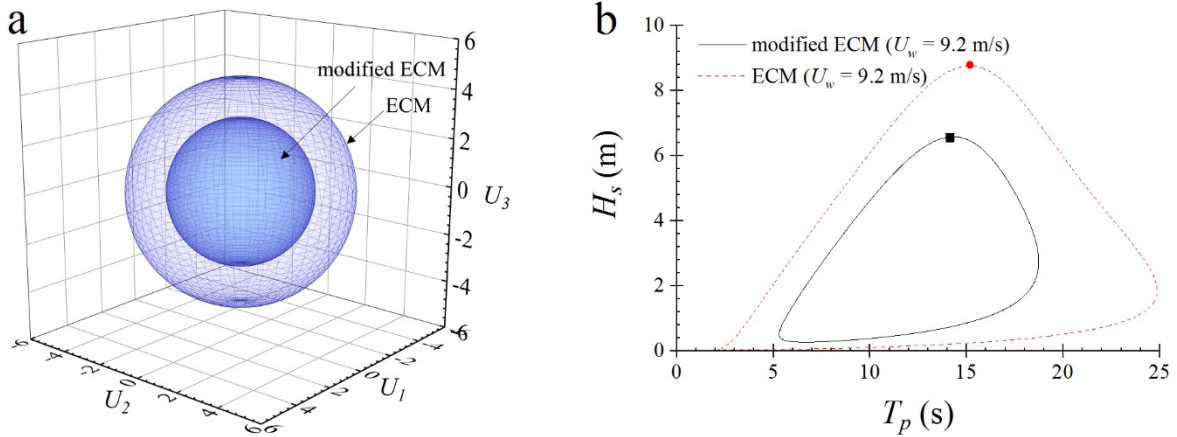


Fig. 14. Selection of contour surface.

326
327

328 Based on the first step of modified ECM, three contour surfaces are identified whereas the ECM still
329 seeks the critical environmental condition from the 50-year one. Fig. 15 shows the critical
330 environmental conditions selected by the two methods. Since the mooring line tension is dominated by
331 the wind force, these two methods both identify $U_w = 9.2$ m/s as the critical wind speed. Nevertheless,
332 the combination of significant wave height and spectrum period picked by these two methods are quite
333 different. The modified ECM selects $H_s = 6.3$ m, $T_p = 14.2$ s as the critical environmental condition
334 whereas the critical parameters identified by the ECM is $H_s = 8.75$ m, $T_p = 15.0$ s. This is because the
335 two select environmental conditions from different contours. Apparently, the ECM selects a rarer wave
336 condition.



337
338
339

Fig. 15. The selected critical environmental condition. (a) U-space; (b) X-space.

340 Table 8 lists the extreme mooring line tension obtained with the two methods. The critical
341 environmental condition identified by the ECM is far from the real one and the ECM underestimates
342 the extreme response by 10% approximately. It reflects the advantage of the modified ECM against the
343 ECM. For response that purely dominated by wave forces, the short-term extreme response with respect
344 to 0.04-year return period is lower than the 50-year extreme value. Extrapolating the 0.04-year return
345 period extreme to the 50-year value by Eq. (9), the modified ECM may produce similar results with the

346 ECM. But it is not the case for the mooring line tension which is dominated by the wind forces rather
 347 than the wave forces. In fact, a rare wave condition won't increase the extreme tension force much.
 348 When the 0.04-year short-term extreme is extrapolated, the modified ECM will produce a much larger
 349 extreme response.

350 Table 8
 351 Selected critical environmental conditions and extreme mooring line tension

method	Selected environmental parameters			Return period (year)	Extreme (kN)
	U_w (m/s)	H_s (m)	T_p (s)		
modified ECM	9.2	6.3	14.2	0.04	2134
ECM	9.2	8.75	15.0	50	1942

352

353 6. Conclusions

354 This study deals with long-term extreme response of an integrated offshore renewable energy system
 355 combining a floating wind turbine, a wave energy converter and two tidal turbines. For offshore floating
 356 structures subject to wave excitations, the ECM has been validated to produce accurate results.
 357 Nevertheless, it is not applicable to the integrated device in this study due to the non-monotonic
 358 behaviour of the wind turbine. A modified environmental contour method is thus proposed to address
 359 this problem, which is an expansion of the ECM and still a simplification of the inverse first-order
 360 reliability method. Unlike the ECM which seeks the critical environmental condition on the 50-year
 361 contour surface, the modified ECM considers the non-monotonic behaviour of wind turbine by checking
 362 multiple contour surfaces. The extra contour surfaces are selected based on important wind speeds, at
 363 which the non-monotonic performance of the wind turbine is most remarkable. For the extreme mooring
 364 line tension force, the critical environmental selected by the modified ECM is located on the 0.04-year
 365 contour surface rather than the 50-year one and the modified ECM suggests an extreme value 10%
 366 larger than that given by the ECM. It implies that the critical environmental condition identified by the
 367 modified ECM is closer to the real one.

368 Acknowledgement

369 The authors would like to acknowledge China Scholarship Council for the financial support (No.
 370 201506230127).

371 References

- 372 [1] L. Li, Z. Yuan, Y. Gao, X. Zhang, Wave force prediction effect on the energy absorption of a wave
 373 energy converter with real-time control, IEEE T Sustain Energy (2018) 1-1.
 374 [2] L. Li, Y. Gao, Z.Q. Hu, Z.M. Yuan, S. Day, H.R. Li, Model test research of a semisubmersible
 375 floating wind turbine with an improved deficient thrust force correction approach, Renew Energ 119
 376 (2018) 95-105.

- 377 [3] B. Whitby, C.E. Ugalde-Loo, Performance of Pitch and Stall Regulated Tidal Stream Turbines,
378 IEEE T Sustain Energ 5(1) (2014) 64-72.
- 379 [4] L. Li, Z. Hu, J. Wang, Q. Hu, Dynamic Responses of a Semi-type Offshore Floating Wind Turbine,
380 33rd International Conference on Ocean, Offshore and Arctic Engineering, American Society of
381 Mechanical Engineers, 2014.
- 382 [5] L. Li, Y. Liu, Z. Yuan, Y. Gao, Wind field effect on the power generation and aerodynamic
383 performance of offshore floating wind turbines, Energy 157 (2018) 379-390.
- 384 [6] M.H. Nehrir, C. Wang, K. Strunz, H. Aki, R. Ramakumar, J. Bing, Z. Miao, Z. Salameh, A Review
385 of Hybrid Renewable/Alternative Energy Systems for Electric Power Generation: Configurations,
386 Control, and Applications, IEEE T Sustain Energ 2(4) (2011) 392-403.
- 387 [7] A. Aubault, M. Alves, A. Sarmiento, D. Roddier, A. Peiffer, Modeling of an oscillating water column
388 on the floating foundation WindFloat, International Conference on Ocean, Offshore and Arctic
389 Engineering, American Society of Mechanical Engineers, 2011, pp. 235-246.
- 390 [8] M.J. Muliawan, M. Karimirad, T. Moan, Dynamic response and power performance of a combined
391 spar-type floating wind turbine and coaxial floating wave energy converter, Renew Energ 50 (2013)
392 47-57.
- 393 [9] L. Wan, Z. Gao, T. Moan, Experimental and numerical study of hydrodynamic responses of a
394 combined wind and wave energy converter concept in survival modes, Coast Eng 104 (2015) 151-169.
- 395 [10] L. Wan, M. Greco, C. Lugni, Z. Gao, T. Moan, A combined wind and wave energy-converter
396 concept in survival mode: Numerical and experimental study in regular waves with a focus on water
397 entry and exit, Appl Ocean Res 63 (2017) 200-216.
- 398 [11] L. Wan, Z. Gao, T. Moan, C. Lugni, Experimental and numerical comparisons of hydrodynamic
399 responses for a combined wind and wave energy converter concept under operational conditions, Renew
400 Energ 93 (2016) 87-100.
- 401 [12] C. Michailides, C. Luan, Z. Gao, T. Moan, Effect of flap type wave energy converters on the
402 response of a semi-submersible wind turbine in operational conditions, International Conference on
403 Ocean, Offshore and Arctic Engineering, American Society of Mechanical Engineers, 2014, pp.
404 V09BT09A014-V09BT09A014.
- 405 [13] L. Li, Y. Gao, Z.M. Yuan, S. Day, Z.Q. Hu, Dynamic response and power production of a floating
406 integrated wind, wave and tidal energy system, Renew Energ 116 (2018) 412-422.
- 407 [14] L. Li, Z. Cheng, Z. Yuan, Y. Gao, Short-term extreme response and fatigue damage of an integrated
408 offshore renewable energy system, Renew Energ 126 (2018) 617-629.
- 409 [15] E.E. Bachynski, T. Moan, Point absorber design for a combined wind and wave energy converter
410 on a tension-leg support structure, International Conference on Ocean, Offshore and Arctic Engineering,
411 American Society of Mechanical Engineers, 2013, pp. V008T09A025-V008T09A025.
- 412 [16] R.G. Coe, C. Michelen, A. Eckert-Gallup, C. Sallaberry, Full long-term design response analysis
413 of a wave energy converter, Renew Energ (2017).

- 414 [17] P. Agarwal, L. Manuel, Simulation of offshore wind turbine response for long-term extreme load
415 prediction, *Eng Struct* 31(10) (2009) 2236-2246.
- 416 [18] P. Videiro, T. Moan, Efficient evaluation of long-term distributions, *International Conference on*
417 *Offshore Mechanics and Arctic Engineering (OMAE)*, 1999.
- 418 [19] S.R. Winterstein, T.C. Ude, C.A. Cornell, P. Bjerager, S. Haver, Environmental parameters for
419 extreme response: Inverse FORM with omission factors, *Proceedings of the ICOSAR-93*, Innsbruck,
420 Austria (1993) 551-557.
- 421 [20] Y. Xiang, Y. Liu, Application of inverse first-order reliability method for probabilistic fatigue life
422 prediction, *Probabilistic Engineering Mechanics* 26(2) (2011) 148-156.
- 423 [21] L. Li, Z. Gao, T. Moan, Joint distribution of environmental condition at five european offshore
424 sites for design of combined wind and wave energy devices, *Journal of Offshore Mechanics and Arctic*
425 *Engineering* 137(3) (2015) 031901.
- 426 [22] D. Karmakar, H. Bagbanci, C.G. Soares, Long-Term Extreme Load Prediction of Spar and
427 Semisubmersible Floating Wind Turbines Using the Environmental Contour Method, *Journal of*
428 *Offshore Mechanics and Arctic Engineering* 138(2) (2016) 021601.
- 429 [23] J. Canning, P. Nguyen, L. Manuel, R.G. Coe, On the Long-Term Reliability Analysis of a Point
430 Absorber Wave Energy Converter, *International Conference on Ocean, Offshore and Arctic*
431 *Engineering*, American Society of Mechanical Engineers, 2017, pp. V010T09A024-V010T09A024.
- 432 [24] K. Saranyasontorn, L. Manuel, On assessing the accuracy of offshore wind turbine reliability-
433 based design loads from the environmental contour method, *International Journal of Offshore and Polar*
434 *Engineering* 15(02) (2005).
- 435 [25] K. Saranyasontorn, L. Manuel, Efficient models for wind turbine extreme loads using inverse
436 reliability, *J Wind Eng Ind Aerod* 92(10) (2004) 789-804.
- 437 [26] N. Aggarwal, R. Manikandan, N. Saha, Nonlinear short term extreme response of spar type floating
438 offshore wind turbines, *Ocean Eng* 130 (2017) 199-209.
- 439 [27] J.M. Jonkman, Definition of the Floating System for Phase IV of OC3, *Citeseer* 2010.
- 440 [28] L. Li, Z.Q. Hu, J. Wang, Y. Ma, Development and Validation of an Aero-hydro Simulation Code
441 for Offshore Floating Wind Turbine, *J Ocean Wind Energy* 2(1) (2015) 1-11.
- 442 [29] NWTC Information Portal. (WEC-Sim), 2017. <https://nwtc.nrel.gov/WEC-Sim>. (Accessed 15-
443 September 2017).
- 444 [30] A.R. Bramwell, D. Balmford, G. Done, *Bramwell's helicopter dynamics*, Butterworth-
445 Heinemann 2001.
- 446 [31] J.M. Jonkman, M.L. Buhl Jr, *FAST User's Guide*, National Renewable Energy Laboratory (NREL),
447 2005.
- 448 [32] B.J. Koo, A.J. Goupee, R.W. Kimball, K.F. Lambrakos, Model Tests for a Floating Wind Turbine
449 on Three Different Floaters, *J Offshore Mech Arct* 136(2) (2014) 020907.
- 450

A modified environmental contour method is presented.

The modified method identifies multiple environmental contours.

Extreme responses of an integrated offshore renewable energy system are examined.

The modified method has a higher estimation accuracy.

ACCEPTED MANUSCRIPT